Proceedings of the Eighteenth International Conference on
Civil, Structural and Environmental Engineering Computing
Edited by: P. Iványi, J. Kruis and B.H.V. Topping
Civil-Comp Conferences, Volume 10, Paper 10.2
Civil-Comp Press, Edinburgh, United Kingdom, 2025
ISSN: 2753-3239, doi: 10.4203/ccc.10.10.2

An Ordinary State-Based Peridynamic Model for the Simulation of Anisotropic Materials Under Finite Deformation

F. Scabbia, M. Zaccariotto and U. Galvanetto

Department of Industrial Engineering, Università degli Studi di Padova, Italy

Abstract

The theory of peridynamics has been proven to be effective in several applications involving fracture phenomena. Over the past two decades, several works investigated the possibility of modeling anisotropic materials with the peridynamic theory. In this context, we introduced an ordinary state-based peridynamic formulation capable of accurately predicting the anisotropic behavior of materials subjected to small deformations. In this formulation, the stiffness of a bond between two material points depends not only on its own direction (through the single-bond micromodulus), but also on the direction of the other bonds connected to those points (through the double-bond micromodulus). The present work verifies that this peridynamic model can also be applied to anisotropic materials under finite deformations. Furthermore, we developed a numerical method based on an incremental-iterative analysis which is able to solve the geometrically nonlinear problem of Cook's membrane made of a linear, elastic, anisotropic material. This is a preliminary step towards using peridynamic theory to model fracture in hyperelastic anisotropic materials.

Keywords: ordinary state-based peridynamics, anisotropic materials, finite deformation, Cook's membrane, single-bond micromodulus, double-bond micromodulus

1 Introduction

Peridynamics is a nonlocal continuum theory capable of modeling fracture phenomena without any mathematical inconsistencies across the discontinuities in the displacement field [1, 2]. In fact, the displacement gradient used to define the deformation of the body is replaced by integrals over a spherical region with a finite radius. The integration region is called *neighborhood* and the peridynamic interaction between two material points is named *bond*. The forces arising in the bond due to the deformation of the body can be defined to depend only on the relative displacements of the material points, such as in bond-based peridynamics, or on the relative displacements of all material points within the neighborhood, such as in state-based peridynamics. In the former case, the force that one point exerts on another is the same as the force that the second point exerts on the first one. However, since the bond force is defined by a pair potential function in the bond-based formulation, the value of the Poisson's ratio cannot be arbitrarily chosen [3]. On the other hand, in state-based peridynamics the two forces that material points exert on one another may have different magnitudes. This allows to freely choose the value of the Poisson's ratio in these peridynamic models.

Constitutive modeling has been a very active topic of research in the peridynamic community. We focus here on the modeling of anisotropic materials given the role they play in many application fields, such as the medical field (anisotropic biomaterials) and the aerospace industry (advanced composites). The peridynamic stiffness of a bond, called *micromodulus*, can be modified to depend on the direction of the bond itself. This approach was applied to bond-based peridynamics to model materials with anisotropic properties [4, 5]. However, anisotropic materials cannot be accurately modeled by bond-based peridynamics because the elastic coefficients must satisfy Cauchy's relations and at least one of them has a fixed value [5].

A peridynamic material is *ordinary* if the bond forces are always aligned to the bond itself. Bond-based peridynamics [1] and ordinary state-based peridynamics [2] exhibit this characteristic. We proposed an ordinary state-based formulation to model anisotropic materials in [10]. This formulation adopts a micromodulus that depends only on the direction of the bond and an additional micromodulus that depends on the directions of two bonds within the same neighborhood. The former micromodulus, similar to the micromodulus used in bond-based peridynamics, is called *single-bond micromodulus* and the latter, used to overcome Cauchy's relations, is called *double-bond micromodulus*. These micromoduli can be defined in such a way that the peridynamic constitutive laws exactly reproduce all components of the elasticity tensor, regardless of their values.

Another approach to model anisotropic behavior is to consider non-ordinary peridynamic materials. For example, bond-based peridynamics can be enhanced by including shear deformability of the bonds [6] and this allows to overcome the restrictions due to Cauchy's relations when modeling anisotropic materials [7]. Furthermore, the non-ordinary state-based peridynamic formulation can be used to incorporate, without any calibration of the stiffness properties, the constitutive models of

anisotropic materials [2]. However, a stabilization method is required to avoid zero-energy modes in non-ordinary state-based peridynamics [8, 9].

The ordinary state-based formulation proposed in [10] was analyzed under the assumption of small deformations. However, since balance of angular momentum is always satisfied with ordinary material models, it could also be applied to problems with finite deformations without any internal inconsistency or violation of the conservation laws. Therefore, in this work, we verify that the above-mentioned ordinary state-based peridynamic formulation for anisotropic materials is able to solve problems of linear elastic materials under finite deformation. To do so, we develop the numerical method to simulate the 2D benchmark problem of Cook's membrane. Even if materials under large deformation are likely to behave nonlinearly, we restrict our present work to linear materials. However, this represents the first step towards the simulation of nonlinear, elastic, anisotropic materials under finite deformations.

2 Ordinary state-based peridynamic formulation for anisotropic materials under finite deformations

By convention, a peridynamic state is denoted with underline and the bond to which the state is applied is denoted within angle brackets $\langle\cdot\rangle$ [2]. Let us consider, for example, a bond $\boldsymbol{\xi} = \mathbf{x}' - \mathbf{x}$ between the material points $\mathbf{x}$ and $\mathbf{x}'$. The *displacement vector state* describes the relative displacement of the bond and is defined as

$$\underline{\mathbf{U}}\langle\boldsymbol{\xi}\rangle = \mathbf{u}(\mathbf{x}') - \mathbf{u}(\mathbf{x})\,, \tag{1}$$

where $\mathbf{u}$ is a displacement field. The *extension scalar state* describes the axial elongation of the bond and is defined as

$$\underline{e}\langle\boldsymbol{\xi}\rangle = \|\boldsymbol{\xi} + \underline{\mathbf{U}}\langle\boldsymbol{\xi}\rangle\| - \|\boldsymbol{\xi}\|\,. \tag{2}$$

The *direction vector state* is the unit vector state in the direction of the deformed bond and is defined as

$$\underline{\mathbf{M}}\langle\boldsymbol{\xi}\rangle = \frac{\boldsymbol{\xi} + \underline{\mathbf{U}}\langle\boldsymbol{\xi}\rangle}{\|\boldsymbol{\xi} + \underline{\mathbf{U}}\langle\boldsymbol{\xi}\rangle\|}\,. \tag{3}$$

Peridynamics is based on integrals that sum up the contributions of all bonds connected to a point. For instance, the internal force acting on a point $\mathbf{x}$ is computed as the integral of forces of the bonds connected to point $\mathbf{x}$. In fact, the peridynamic equilibrium equation in static conditions is given as

$$-\int_{\mathcal{H}_\mathbf{x}} \left(\underline{\mathbf{T}}\langle\boldsymbol{\xi}\rangle - \underline{\mathbf{T}}\langle-\boldsymbol{\xi}\rangle\right) \mathrm{d}V_{\mathbf{x}'} = \mathbf{b}(\mathbf{x})\,. \tag{4}$$

where $\underline{\mathbf{T}}$ is the force vector state (force per unit volume squared), $\mathcal{H}_\mathbf{x}$ is the neighborhood of point $\mathbf{x}$, $V_{\mathbf{x}'}$ is the volume of point $\mathbf{x}'$, and $\mathbf{b}$ is the external force density. In 2D models, the neighborhood is often chosen to be a circle with a radius δ, named the

horizon size. The force state for the peridynamic model for anisotropic materials is defined in Eq. (8).

For later use, the *weighted volume* at a point $\mathbf{x}$ is defined as

$$m(\mathbf{x}) = \int_{\mathcal{H}_\mathbf{x}} \underline{\omega}\langle \boldsymbol{\xi} \rangle \, \|\boldsymbol{\xi}\|^2 \, \mathrm{d}V_{\mathbf{x}'} \,, \tag{5}$$

where $\underline{\omega}$ is a scalar state called *influence function*. In this work, the influence function is chosen as $\underline{\omega}\langle \boldsymbol{\xi} \rangle = 1$ and does not explicitly appear in the following peridynamic integrals.

2.1 Constitutive model

In bond-based peridynamics for anisotropic materials, the stiffness of a bond depends on the direction of that bond. The scalar state that describes this bond stiffness is denoted by $\underline{k}\langle \boldsymbol{\xi} \rangle$, namely the *single-bond micromodulus*. Since bond-based models are based on pairwise interactions, they must satisfy Cauchy's relations [5]. In fcat, in a 2D problem involving a bond-based peridynamic material, if 5 out of 6 independent components of the elasticity tensor are chosen, the sixth component is fixed due to Cauchy's relation.

Let us now consider two bonds connected to a material point $\mathbf{x}$, namely $\boldsymbol{\xi} = \mathbf{x}' - \mathbf{x}$ and $\boldsymbol{\zeta} = \mathbf{x}'' - \mathbf{x}$, where the points $\mathbf{x}'$ and $\mathbf{x}''$ lie within the neighborhood of point $\mathbf{x}$ as shown in Figure 1. To overcome the limitation due to Cauchy's relations, an additional bond stiffness that depends on the directions of pairs of bonds, such as the pair $\boldsymbol{\xi}$ and $\boldsymbol{\zeta}$, can be included in the formulation. The scalar double state that describes this bond stiffness is denoted by $\underline{\lambda}\langle \boldsymbol{\xi}, \boldsymbol{\zeta} \rangle$ and is called *double-bond micromodulus*. This micromodulus must satisfy $\underline{\lambda}\langle \boldsymbol{\xi}, \boldsymbol{\zeta} \rangle = \underline{\lambda}\langle \boldsymbol{\zeta}, \boldsymbol{\xi} \rangle$ to ensure that the peridynamic elasticity tensor possesses the major symmetry. Therefore, in the ordinary state-based peridynamic formulation for anisotropic materials, the stiffness of a bond $\boldsymbol{\xi}$ depends not only on its direction but also on the directions of the bonds (like $\boldsymbol{\zeta}$) connected to point $\mathbf{x}$ [10].

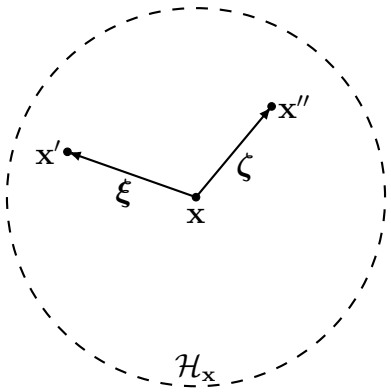

Figure 1: *Two bonds connected to point* $\mathbf{x}$.

In order to model general anisotropic properties in ordinary state-based peridynamics, a new definition of strain energy density at a point $\mathbf{x}$ is introduced [10]:

$$W(\mathbf{x}) = \frac{1}{2\,m(\mathbf{x})} \int_{\mathcal{H}_\mathbf{x}} \underline{k}\langle\boldsymbol{\xi}\rangle \left(\underline{e}\langle\boldsymbol{\xi}\rangle\right)^2 \mathrm{d}V_{\mathbf{x}'} + \frac{1}{2\,m(\mathbf{x})} \int_{\mathcal{H}_\mathbf{x}} \|\boldsymbol{\xi}\|\, \underline{e}\langle\boldsymbol{\xi}\rangle\, \underline{\Lambda}\langle\boldsymbol{\xi}\rangle \,\mathrm{d}V_{\mathbf{x}'}\,, \tag{6}$$

where $\underline{\Lambda}\langle\boldsymbol{\xi}\rangle$ is a scalar state named *microforce*, which is computed as

$$\underline{\Lambda}\langle\boldsymbol{\xi}\rangle = \frac{1}{m(\mathbf{x})} \int_{\mathcal{H}_\mathbf{x}} \underline{\lambda}\langle\boldsymbol{\xi},\boldsymbol{\zeta}\rangle\, \|\boldsymbol{\zeta}\|\, \underline{e}\langle\boldsymbol{\zeta}\rangle \,\mathrm{d}V_{\mathbf{x}''}\,. \tag{7}$$

Since the contribution of the bond $\boldsymbol{\zeta}$ is integrated over the neighborhood of point $\mathbf{x}$, the microforce depends only on the bond $\boldsymbol{\xi}$. The definition of the microforce is similar to that of dilatation in the original ordinary state-based formulation, but it also embeds information about the stiffness of the bond related to the double-bond micromodulus. If the material is isotropic, the micromoduli are constant for any direction of the bond and an ordinary state-based peridynamic formulation for isotropic materials is retrieved.

From the derivatives of the strain energy density in Eq. (6), the force density vector state and the components of the elasticity tensor can be respectively obtained (see Appendix A in [10] for details) as

$$\underline{\mathbf{T}}\langle\boldsymbol{\xi}\rangle = \frac{1}{m(\mathbf{x})} \left[\underline{k}\langle\boldsymbol{\xi}\rangle\, \underline{e}\langle\boldsymbol{\xi}\rangle + \|\boldsymbol{\xi}\|\, \underline{\Lambda}\langle\boldsymbol{\xi}\rangle\right] \underline{\mathbf{M}}\langle\boldsymbol{\xi}\rangle\,, \tag{8}$$

$$\begin{aligned} C_{ijk\ell}(\mathbf{x}) = \frac{1}{m(\mathbf{x})} \int_{\mathcal{H}_\mathbf{x}} \underline{k}\langle\boldsymbol{\xi}\rangle \frac{\xi_i\xi_j\xi_k\xi_\ell}{\|\boldsymbol{\xi}\|^2} \,\mathrm{d}V_{\mathbf{x}'} \\ + \frac{1}{(m(\mathbf{x}))^2} \int_{\mathcal{H}_\mathbf{x}} \int_{\mathcal{H}_\mathbf{x}} \underline{\lambda}\langle\boldsymbol{\xi},\boldsymbol{\zeta}\rangle\, \xi_i\xi_j\zeta_k\zeta_\ell \,\mathrm{d}V_{\mathbf{x}''}\,\mathrm{d}V_{\mathbf{x}'}\,. \end{aligned} \tag{9}$$

Note that the second term in Eq. (9) allows to overcome the restrictions due to Cauchy's relations, which instead would be inevitably present if only the first term was used. In fact, in the latter case, the order of the indices would be irrelevant and the peridynamic material would be required to satisfy Cauchy's relations ($C_{ijk\ell} = C_{ikj\ell}$).

In this work, we consider only 2D problems and we adopt the same functions that were used in [10] (even if their choice is not univocal) to describe the variation of the micromoduli with the directions of the bonds:

$$\underline{k}\langle\boldsymbol{\xi}\rangle = \frac{1}{\|\boldsymbol{\xi}\|^4} \left(k_{xxxx}\,\xi_x^4 + k_{xxxy}\,\xi_x^3\xi_y + k_{xxyy}\,\xi_x^2\xi_y^2 + k_{yyxy}\,\xi_x\xi_y^3 + k_{yyyy}\,\xi_y^4\right)\,, \tag{10}$$

$$\underline{\lambda}\langle\boldsymbol{\xi},\boldsymbol{\zeta}\rangle = \frac{1}{\|\boldsymbol{\xi}\|^2\|\boldsymbol{\zeta}\|^2}\, \lambda_{xyxy}\,\xi_x\xi_y\zeta_x\zeta_y\,. \tag{11}$$

The constants in these equations are determined by substituting Eq. (10) and Eq. (11) into Eq. (9) and computing the integrals for the 6 independent components of the elasticity tensor. This calibration is used to match the components of the elasticity tensor

obtained with ordinary state-based peridynamics with those of classical continuum mechanics:

$$k_{xxxx} = 5C_{xxxx} - 10C_{xxyy} + C_{yyyy}\,, \tag{12a}$$
$$k_{xxxy} = 40C_{xxxy} - 24C_{yyxy}\,, \tag{12b}$$
$$k_{xxyy} = 76C_{xxyy} - 10C_{xxxx} - 10C_{yyyy}\,, \tag{12c}$$
$$k_{yyxy} = 40C_{yyxy} - 24C_{xxxy}\,, \tag{12d}$$
$$k_{yyyy} = 5C_{yyyy} - 10C_{xxyy} + C_{xxxx}\,, \tag{12e}$$
$$\lambda_{xyxy} = 64C_{xyxy} - 64C_{xxyy}\,. \tag{12f}$$

Note that, depending on the values of the components of the elasticity tensor, some constants may be negative resulting in possible instabilities of the model. Furthermore, since Eq. (9) is valid only in the linearized case of small deformations [10], the calibration of the micromoduli is approximated for the case of finite deformations and may result in high discrepancies with respect to classical models for very large deformations. Another cause of differences between the peridynamic and classical models is the so-called *surface effect*, which is due to the fact that the calibration of the peridynamic micromoduli is carried out assuming a complete neighborhood, whereas peridynamic points close to the boundary of the body have an incomplete neighborhood [11–14].

2.2 Numerical method

In order to solve a load-controlled problem with geometrical nonlinearity due to finite deformations, an incremental-iterative analysis can be carried out: the external load is incrementally applied in steps and the solution after the application of each increment is obtained (within a chosen tolerance) with an iterative procedure, such as the Newton-Raphson method [15]. If the internal and external force vectors are denoted by $\mathbf{f}_{\text{int}}$ and $\mathbf{f}_{\text{ext}}$, an increment in the external force vector $\Delta\mathbf{f}_{\text{ext}}$ results in an increment in the displacement field $\Delta\mathbf{u}$. Thanks to the Newton-Raphson method within the step, the equations can be linearized as

$$\mathbf{f}_{\text{int}} + \mathbf{K}\,\Delta\mathbf{u} = \mathbf{f}_{\text{ext}} + \Delta\mathbf{f}_{\text{ext}}\,, \tag{13}$$

where $\mathbf{K}$ is the tangent stiffness matrix. The increment of the displacement field $\Delta\mathbf{u}$ can be determined by solving Eq. (13). The new internal force vector can be computed with the displacement vector $\mathbf{u} + \Delta\mathbf{u}$ and compared with the external force vector $\mathbf{f}_{\text{ext}} + \Delta\mathbf{f}_{\text{ext}}$ to compute the relative residual:

$$r = \frac{\|\mathbf{f}_{\text{ext}} + \Delta\mathbf{f}_{\text{ext}} - \mathbf{f}_{\text{int}}\|}{\|\mathbf{f}_{\text{ext}} + \Delta\mathbf{f}_{\text{ext}}\|}\,, \tag{14}$$

If this residual is less than the prescribed tolerance, the external load can be incremented again. Otherwise, a new iteration of the Newton-Raphson method is carried out. In this work, the tolerance is chosen as 10^{-6}.

The meshfree method with a regular grid of nodes is often used to discretize peridynamic models [16]. In 2D models, each node represents a square area h^2 with thickness t, where h is the grid spacing. The peridynamic equilibrium equation at a node p for an increment in the external load is discretized as

$$-\sum_{q\in\mathcal{H}_p}\left(\underline{\mathbf{T}}_{pq}-\underline{\mathbf{T}}_{qp}+\Delta\underline{\mathbf{T}}_{pq}-\Delta\underline{\mathbf{T}}_{qp}\right)\,\beta_{pq}\,t^2\,h^4=\left(\mathbf{b}_p+\Delta\mathbf{b}_p\right)t\,h^2\,. \tag{15}$$

where $\mathcal{H}_p$ is the neighborhood of node p, $\underline{\mathbf{T}}_{pq}=\underline{\mathbf{T}}\langle\boldsymbol{\xi}_{pq}\rangle$ and $\underline{\mathbf{T}}_{qp}=\underline{\mathbf{T}}\langle\boldsymbol{\xi}_{qp}\rangle$ are the force states of the bonds between nodes p and q, β_{pq} is the quadrature coefficient, and $\mathbf{b}_p$ is the external force density acting on node p. The quadrature coefficient β, used to improve the numerical results of the integration, is computed with the algorithm developed in [17]. By comparing Eq. (13) with Eq. (15), the following relations can be derived:

$$\mathbf{f}_{\text{ext}}+\Delta\mathbf{f}_{\text{ext}}=\left(\mathbf{b}_p+\Delta\mathbf{b}_p\right)t\,h^2\,, \tag{16}$$

$$\mathbf{f}_{\text{int}}=-\sum_{q\in\mathcal{H}_p}\left(\underline{\mathbf{T}}_{pq}-\underline{\mathbf{T}}_{qp}\right)\,\beta_{pq}\,t^2\,h^4\,, \tag{17}$$

$$\mathbf{K}\,\Delta\mathbf{u}=-\sum_{q\in\mathcal{H}_p}\left(\Delta\underline{\mathbf{T}}_{pq}-\Delta\underline{\mathbf{T}}_{qp}\right)\,\beta_{pq}\,t^2\,h^4\,. \tag{18}$$

To evaluate the force state at the previous iteration and its increment, the following equations are required:

$$\underline{\mathbf{U}}_{pq}+\Delta\underline{\mathbf{U}}_{pq}=\mathbf{u}_q-\mathbf{u}_p+\Delta\mathbf{u}_q-\Delta\mathbf{u}_p\,, \tag{19}$$

$$\underline{\mathbf{M}}_{pq}+\Delta\underline{\mathbf{M}}_{pq}\approx\frac{\boldsymbol{\xi}_{pq}+\underline{\mathbf{U}}_{pq}}{\|\boldsymbol{\xi}_{pq}+\underline{\mathbf{U}}_{pq}\|}+\frac{\Delta\underline{\mathbf{U}}_{pq}}{\|\boldsymbol{\xi}_{pq}+\underline{\mathbf{U}}_{pq}\|}\,, \tag{20}$$

$$\underline{e}_{pq}+\Delta\underline{e}_{pq}\approx\|\boldsymbol{\xi}_{pq}+\underline{\mathbf{U}}_{pq}\|-\|\boldsymbol{\xi}_{pq}\|+\underline{\mathbf{M}}_{pq}\cdot\Delta\underline{\mathbf{U}}_{pq}\,, \tag{21}$$

$$m_p=\sum_{q\in\mathcal{H}_p}\|\boldsymbol{\xi}_{pq}\|^2\,\beta_{pq}\,t\,h^2\,, \tag{22}$$

$$\underline{\Lambda}_{pq}+\Delta\underline{\Lambda}_{pq}=\frac{1}{m_p}\sum_{r\in\mathcal{H}_p}\underline{\lambda}_{pq,pr}\,\|\boldsymbol{\zeta}_{pr}\|\,\underline{e}_{pr}\,\beta_{pr}\,t\,h^2 + \frac{1}{m_p}\sum_{r\in\mathcal{H}_p}\underline{\lambda}_{pq,pr}\,\|\boldsymbol{\zeta}_{pr}\|\,\Delta\underline{e}_{pr}\,\beta_{pr}\,t\,h^2\,, \tag{23}$$

$$\underline{\mathbf{T}}_{pq}+\Delta\underline{\mathbf{T}}_{pq}=\frac{1}{m_p}\left[\underline{k}_{pq}\left(\underline{e}_{pq}+\Delta\underline{e}_{pq}\right)+\|\boldsymbol{\xi}_{pq}\|\left(\underline{\Lambda}_{pq}+\Delta\underline{\Lambda}_{pq}\right)\right]\left(\underline{\mathbf{M}}_{pq}+\Delta\underline{\mathbf{M}}_{pq}\right)\,, \tag{24}$$

where the symbol "$\approx$" means that the equation was linearized with respect to the increment $\Delta\mathbf{u}$. Therefore, the force state at the previous iteration, used to compute the internal force vector in Eq. (17), is given as

$$\underline{\mathbf{T}}_{pq}=\frac{1}{m_p}\left[\underline{k}_{pq}\,\underline{e}_{pq}+\|\boldsymbol{\xi}_{pq}\|\,\underline{\Lambda}_{pq}\right]\underline{\mathbf{M}}_{pq}\,, \tag{25}$$

whereas the increment in the force state, used to compute the tangent stiffness matrix in Eq. (18), is given as

$$\Delta\underline{\mathbf{T}}_{pq} \approx \frac{1}{m_p}\left[\underline{k}_{pq}\,\Delta\underline{e}_{pq} + \|\boldsymbol{\xi}_{pq}\|\,\Delta\underline{\Lambda}_{pq}\right]\underline{\mathbf{M}}_{pq} + \frac{1}{m_p}\left[\underline{k}_{pq}\,\underline{e}_{pq} + \|\boldsymbol{\xi}_{pq}\|\,\underline{\Lambda}_{pq}\right]\Delta\underline{\mathbf{M}}_{pq}\,. \tag{26}$$

With these equations, it is possible to implement the incremental-iterative analysis that, if convergence is reached, finds the solution to the ordinary state-based peridynamic model for anisotropic materials under finite deformations.

3 Numerical example

We validate the numerical peridynamic model for anisotropic materials under finite deformations by solving the benchmark problem of Cook's membrane. Figure 2 shows the geometry and boundary conditions imposed to the membrane. The thickness t of the membrane is assumed to be equal to 1 mm. The left edge of the membrane is clamped, whereas a force $\bar{\mathbf{f}} = 5$ kN is applied to the right edge. This load is subdivided into 10 equal increments for the incremental-iterative analysis. The boundary conditions are applied on the most external layer of nodes, even if this approach may lead to undesired fluctuations in the peridynamic solution [12–14].

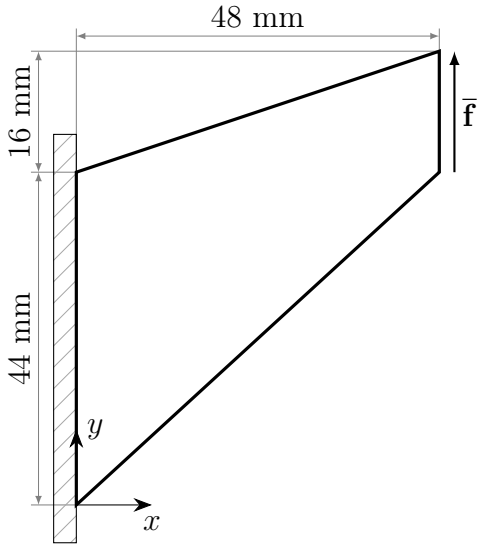

Figure 2: *Geometry and boundary conditions of the benchmark problem of Cook's membrane.*

We define a made-up orthotropic material for this numerical simulation with the following properties: $E_1 = 15$ GPa, $E_2 = 10$ GPa, $G_{12} = 5$ GPa, and $\nu_{12} = 0.35$, where E is the Young's modulus, G is the shear modulus, ν is the Poisson's ratio, and the subscripts indicate the directions in the material reference system. We also assume that the material system is rotated by $\phi = 10^\circ$ anticlockwise with respect to the problem reference system to obtain a full elasticity matrix with the following

components (see Section 6.1 of [10] for details of these calculations): $C_{xxxx} = 16.18$ GPa, $C_{yyyy} = 11.07$ GPa, $C_{xxyy} = 3.80$ GPa, $C_{xyxy} = 4.99$ GPa, $C_{xxxy} = 0.43$ GPa, $C_{yyxy} = 0.50$ GPa.

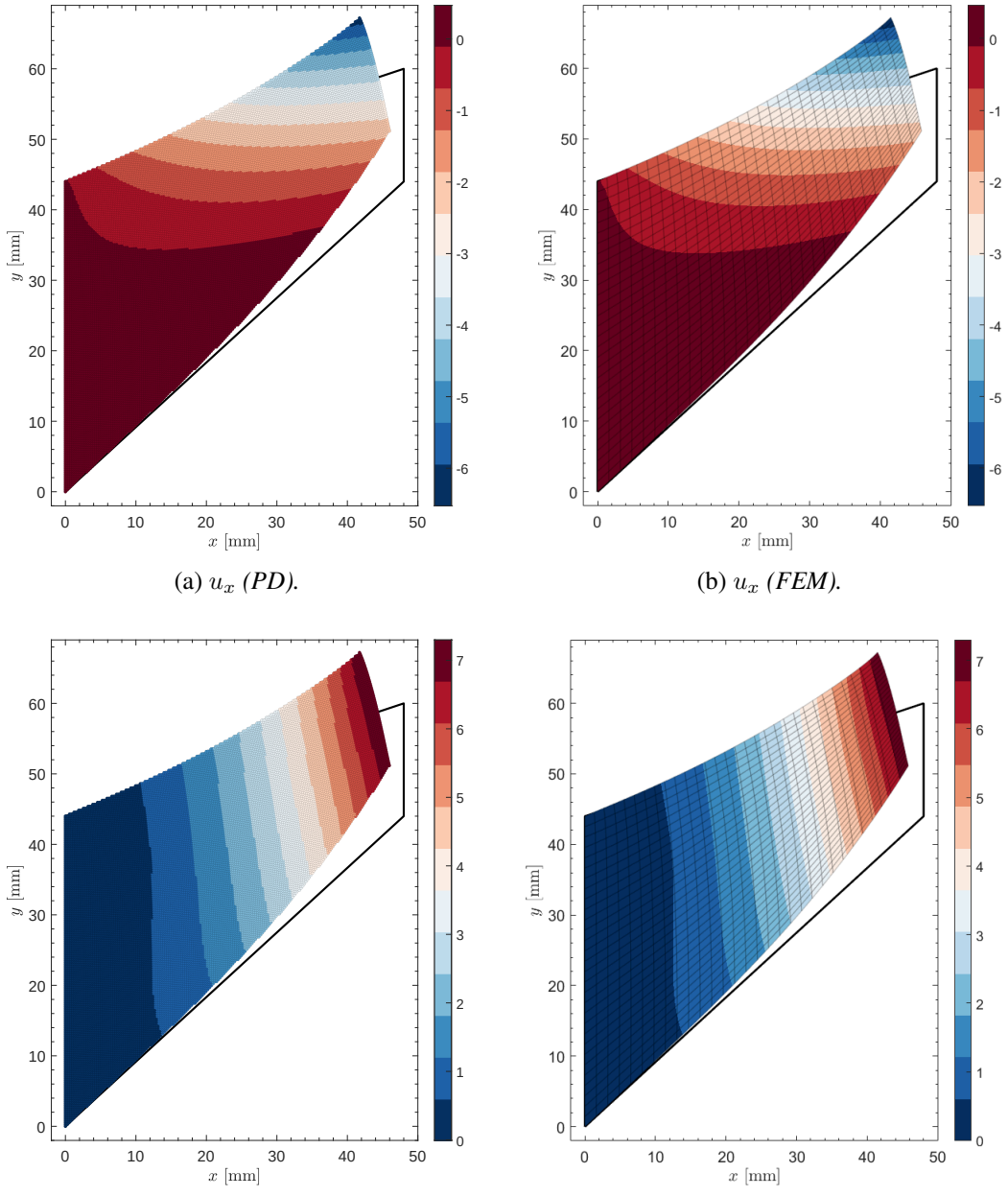

(a) u_x *(PD).* (b) u_x *(FEM).*

(c) u_y *(PD).* (d) u_y *(FEM).*

Figure 3: *Displacement field obtained with peridynamics (PD) and finite element method (FEM) for the problem of Cook's membrane.*

The peridynamic body is discretized with a uniform grid spacing $h = 0.25$ mm and the horizon size is $\delta = 0.75$ mm. The same problem is also solved with the finite element method (FEM) to provide a comparison with a solution obtained with

classical continuum mechanics. For this simulation 8-node bilinear elements are used, 30 of them in each of the two direction. The results obtained with the two methods are shown in Figure 3.

As discussed before, the PD and FEM solutions are not the same because they are obtained with a nonlocal theory and a local theory, respectively. However, since δ is small enough, the two solutions are similar. For instance, the displacement in x direction of the node at the top right-hand corner of Cook's membrane are $u_x = -6.28$ mm for the PD model and $u_x = -6.53$ mm for the FEM model, whereas the displacement in y direction of that node are $u_y = 7.20$ mm for the PD model and $u_y = 7.22$ mm for the FEM model.

4 Conclusions

The constitutive modeling of anisotropic materials in the peridynamic theory has been the topic of several papers in the last two decades. In particular, the authors of the present work proposed an ordinary state-based peridynamic formulation to accurately model anisotropic materials under small deformations. In this work, we verified that this formulation is valid also in the case of finite deformations. We developed a numerical peridynamic method able to address problems involving linear, elastic, anisotropic materials under finite deformations and proved its validity by solving the benchmark problem of Cook's membrane. The results obtained with this method are similar to those obtained with a classical finite element method. Although materials under large deformation are likely to have a nonlinear constitutive model, we limited the present analysis to geometrically nonlinear problems involving linear materials. Nevertheless, this work represents a first step towards the possibility of modeling hyperelastic anisotropic materials with the peridynamic theory.

Acknowledgements

The authors acknowledge support from the European Union - Next GenerationEU under the call PRIN 2022 PNRR of the Italian Minister of University and Research (MUR); Project P2022HLHHB (PE - Physical Sciences and Engineering) A digital framework for the cutting of soft tissues: A first step towards virtual surgery (National coordinator V.D.), and from University of Padova under the research projects BIRD2023 NR.237212/23 and NR.232492/23.

References

[1] S.A. Silling, "Reformulation of elasticity theory for discontinuities and long-range forces", Journal of the Mechanics and Physics of Solids, 48, 175-209, 2000.

[2] S.A. Silling, M. Epton, O. Weckner, J. Xu, E. Askari, "Peridynamic states and constitutive modeling", Journal of elasticity, 88, 151-184, 2007.

[3] J. Trageser, P. Seleson, "Bond-based peridynamics: a tale of two Poisson's ratios", Journal of Peridynamics and Nonlocal Modeling, 2, 278-288, 2020.

[4] M. Ghajari, L. Iannucci, P. Curtis, "A peridynamic material model for the analysis of dynamic crack propagation in orthotropic media", Computer Methods in Applied Mechanics and Engineering, 276, 431-452, 2014.

[5] J. Trageser, P. Seleson, "Anisotropic two-dimensional, plane strain, and plane stress models in classical linear elasticity and bond-based peridynamics", arXiv preprint, 2019.

[6] V. Diana, S. Casolo, "A bond-based micropolar peridynamic model with shear deformability: Elasticity, failure properties and initial yield domains", International Journal of Solids and Structures, 160, 201-231, 2019.

[7] V. Diana, S. Casolo, "A full orthotropic micropolar peridynamic formulation for linearly elastic solids", International Journal of Mechanical Sciences, 160, 140-155, 2019.

[8] H. Chen, "Bond-associated deformation gradients for peridynamic correspondence model", Mechanics Research Communications, 90, 34-41, 2018.

[9] T. Breitzman, K. Dayal, "Bond-level deformation gradients and energy averaging in peridynamics", Journal of the Mechanics and Physics of Solids, 110, 192-204, 2018.

[10] F. Scabbia, M. Zaccariotto, U. Galvanetto, "A general ordinary state-based peridynamic formulation for anisotropic materials", Computer Methods in Applied Mechanics and Engineering, 427, 117059, 2024.

[11] Q.V. Le, F. Bobaru, "Surface corrections for peridynamic models in elasticity and fracture", Computational Mechanics, 61, 499-518, 2018.

[12] F. Scabbia, M. Zaccariotto, U. Galvanetto, "A novel and effective way to impose boundary conditions and to mitigate the surface effect in state-based Peridynamics", International Journal for Numerical Methods in Engineering, 122, 5773-5811, 2021.

[13] F. Scabbia, M. Zaccariotto, U. Galvanetto, "A new method based on Taylor expansion and nearest-node strategy to impose Dirichlet and Neumann boundary conditions in ordinary state-based Peridynamics", Computational Mechanics, 70, 1-27, 2022.

[14] F. Scabbia, M. Zaccariotto, U. Galvanetto, "A new surface node method to accurately model the mechanical behavior of the boundary in 3D state-based Peridynamics", Journal of Peridynamics and Nonlocal Modeling, 5, 521-555, 2023.

[15] R. De Borst, M.A. Crisfield, J.J. Remmers, C.V. Verhoosel, Nonlinear finite element analysis of solids and structures, John Wiley & Sons, 2012.

[16] S.A. Silling, E. Askari, “A meshfree method based on the peridynamic model of solid mechanics”, Computers & structures, 83, 1526-1535, 2005.
[17] F. Scabbia, M. Zaccariotto, U. Galvanetto, “Accurate computation of partial volumes in 3D peridynamics”, Engineering with Computers, 39, 959-991, 2023.